Bioinspired gold nanoparticles synthesized from Persicaria capitata leaves and their antimicrobial and anticancer activities

Stuti Gupta
Department of Chemistry, Hemvati Nandan Garhwal University, BGR Campus Pauri, (Garhwal) 246001
Reena Purohit
Department of Chemistry, Bal Ganga Mahavidhyalaya, Sandul-Kemar
Shikha Syal
Department of Chemistry, Hemvati Nandan Garhwal University, BGR Campus Pauri, (Garhwal) 246001
Sonali Purohit
Assistant Professor-Consultant Department of Shalakya Tantra, Uttaranchal Medical College of Ayurveda and Research, Premnagar Dehradun
Anuj Kandwal
Department of Chemistry, Harsh Vidya mandir (P.G.) College Raisi, Haridwar, 247671
Archana Bachheti
Department of Environment Science, Graphic Era (Deemed to be University), Dehradun-248002
Rakesh Kumar Bachheti
Centre of Molecular Medicine and Diagnostics, Saveetha Dental College & Hospitals, Saveetha Institute of Medical and Technical Sciences, Saveetha University
Limenew Abate Worku
limenewabate@gmail.com

Debre Tabor University, College of Natural and Computational Science, Department of Chemistry
M.C. Purohit
Department of Chemistry, Hemvati Nandan Garhwal University, BGR Campus Pauri, (Garhwal) 246001

Research Article

Keywords: Gold nanoparticles, Anticancer, antibacterial MTT assay, Persicaria capitata, XRD

Posted Date: January 9th, 2026

DOI: https://doi.org/10.21203/rs.3.rs-8347930/v1

Additional Declarations: No competing interests reported.

Abstract

A green technique that enables one-pot synthesis is the plant-mediated biosynthesis of nanoparticles. Owing to their wide range of applications, the synthesis of gold nanoparticles (AuNPs) using plant extracts has attracted considerable attention in the biomedical field. In this study, the aqueous extract of *Persicaria capitata* leaves was employed to synthesize AuNPs via a green chemistry approach at room temperature. The formation of AuNPs was confirmed by UV–Vis spectroscopy, which showed a surface plasmon resonance peak at 534 nm. XRD analysis indicated the crystalline nature of the nanoparticles, revealing a cubic close-packed (ccp) phase structure. EDX spectra of *P. capitata*-derived AuNPs exhibited weak peaks at around 0.25 keV and 0.5 keV, likely due to biomolecules attached to the nanoparticle surface, along with a sharp, intense signal at 2.1 keV that confirmed the presence of elemental gold. TEM examination showed nanoparticles with both spherical and triangular morphologies and FTIR analysis demonstrated the presence of bioactive molecules responsible for reducing Au^{3+} ions during synthesis. For antimicrobial activity, bacterial cultures were grown on soybean casein digest agar medium and fungal cultures on potato dextrose agar medium. The synthesized AuNPs exhibited inhibitory effects against *Escherichia coli*, *Bacillus subtilis*, *Candida albicans*, and *Aspergillus oryzae*, with zones of inhibition measuring 10.0 mm, 7.0 mm, 15.0 mm, and 10.0 mm, respectively. The anticancer potential of the synthesized AuNPs was evaluated using both in vitro and in vivo experiments. MTT and SRB assays were performed on hepatic (Hep-2) cell lines, while in vivo studies involved induction of cancer in the livers of Swiss albino rats. Parameters such as tumor weight, hemoglobin content, viable and non-viable cells, RBC count, and WBC count were assessed. The results indicated that the AuNPs inhibited cancer cell proliferation and exhibited significant anticancer activity. Future research should focus on elucidating detailed mechanisms, conducting clinical validation, and developing large-scale production strategies to translate these findings into practical biomedical applications.

Introduction

Metallic nanoparticles are among the most versatile nanomaterials, with wide-ranging applications in chemistry, electronics, medicine, and pharmaceutical sciences [1]. Among them, gold nanoparticles (AuNPs) are particularly notable due to their biocompatibility, tunable optical properties, and easily modifiable surface chemistry [2, 3]. Owing to these unique physicochemical features, AuNPs are extensively employed as carriers for drugs and biomolecules, enhancing both disease diagnosis and treatment[4, 5]. Traditional chemical and physical synthesis methods for AuNPs are well established; however, they often involve toxic substances and non-polar solvents, leading to environmental concerns, multiple purification steps, and high production costs [6]. To address these limitations, biosynthetic or “green” synthesis approaches have been developed[7] These methods utilize natural compounds from plants or microorganisms such as fungi, bacteria, and algae as reducing and stabilizing agents in the conversion of gold ions [7, 8]. Green synthesis is considered simple, cost-effective, and environmentally friendly, as it typically employs water and other non-toxic solvents [9]. Reports have demonstrated the successful production of metallic nanoparticles from natural sources, highlighting its potential as a

sustainable alternative[10, 11]. Plant extracts, in particular, are rich in molecules with strong redox activity, including flavonoids, terpenoids, fatty acids, amino acids, aldehydes, and alcohols [12, 13] making them excellent candidates for the biosynthesis of AuNPs Biogenic synthesis produces large amounts of highly stable nanoparticles with better-defined sizes compared to some conventional methods, as the phytochemical compounds used in the reaction also act as stabilizing agents [14, 15]. The large surface area and high proportion of surface atoms of metal nanoparticles make them highly significant. Metal nanoparticles have been widely studied because of their unique chemical and physical characteristics and their importance in science and technology.Gold nanoparticles, in particular, have diverse applications in biosensing [16], catalysis [17], electronics [18], enzyme electrodes [19], superconductors, and cancer therapy[20, 21]. Biological nanoscience has recently gained increasing attention due to its potential biomedical, industrial, and electronic applications, such as bioimaging [22], cancer detection [23], and catalysis [24]. Gold nanoparticles are especially valuable in genetic medicine, DNA identification, and nano-catalysis. Their size has been shown to influence functional performance [25–27]. To meet specific functional requirements, several methods have been developed for synthesizing noble metal nanoparticles of particular shapes and sizes. The use of environmentally friendly biosynthesis techniques has become a prominent area at the intersection of biotechnology and nanotechnology. Biomolecules as reducing agents offer significant advantages over chemical reductants, primarily due to their better biocompatibility [28].

Persicaria capitata (Buch.-Ham. ex D.Don) H.Gross, commonly known as “Kanphuli,” belongs to the family Polygonaceae. Its leaves are 1–6 cm long and 0.7–3 cm broad, with small, scattered hairs and distinctive pink to crimson stripes or spots. The flower spikes are 5–10 mm long and 5–7 mm in diameter. Native to Asia, *P. capitata* has naturalized in parts of North America and Australia. Traditionally, it is used to treat urinary calculi and urinary tract infections, and it exhibits antimicrobial, anti-inflammatory [29], anticancer, and antitumor activities. It is distributed widely across India, Nepal, and China, particularly in Uttarakhand. The plant contains a variety of phytochemicals, including coumarins, anthraquinones, phenylpropanoids, flavonoids, neoflavonoids, triterpenes, lignans, and sesquiterpenes with dialdehyde functional groups. Notably, compounds such as quercetin, kaempferol, taxifolin, gallic acid, vanillic acid, and protocatechuic acid have been reported from the alcoholic extract [30]. Morphologically, *P. capitata* is a spreading, herbaceous plant that can reach up to 5 cm in height, with branches extending over 20 cm. It produces striking white to pink button-like flowers from late summer to mid-fall, which emerge from pink buds. It thrives in subtropical climates and tolerates the high heat of mountainous regions [31]. Inflorescences, approximately 1.5 cm in diameter, consist of numerous small pink flowers that bloom year-round. The species is valued for its ornamental foliage, which features alternating, oblong, hairy leaves with distinct “V”-shaped bands.*P. capitata* is regarded as an invasive species in some countries. However, it has medicinal applications as a stimulant, astringent, diuretic, and vermifuge [32, 33]. It adapts well to semi-shaded or full-sun conditions and prefers clayey or sandy soil enriched with organic matter. Its seeds, dispersed by animals, germinate readily during the wet season, deonstrating dependence on soil moisture [34, 35]. Propagation occurs through seeds, plant division, or

rooted stems (Rohman, 2011). Because of its low growth habit, tolerance to stress, and ornamental appeal, *P. capitata* has potential applications in green roofs, ground covers, and hanging baskets [36, 37]. Within the genus *Persicaria*, both annual and perennial species are cultivated for soil cover and landscape use. Germination occurs within three weeks at 21–27°C, though the species also propagates rapidly via rooted branches in contact with soil [38].

Although *P. capitata* possesses known medicinal properties, its potential in green synthesis of gold nanoparticles is still underexplored. Conventional chemical methods use toxic agents, limiting biocompatibility, whereas phytochemical-mediated synthesis offers a safer alternative[39]. However, there is insufficient evidence on the stability, efficacy, and therapeutic applications of *P. capitata*-derived gold nanoparticles, highlighting the need for systematic investigation.

Material and Methods

Plant collection

Leaves of *P. capitata* were collected from non-protected, non-private, or non-indigenous land Nagdev Forest range in Pauri, Uttarakhand, India (latitude: 30.17° N, longitude: 78.71° E) in December 2022. The collection site was on land that is neither protected, private, nor indigenous. Appropriate prior informed consent was secured from relevant stakeholders. The plant species was identified by Dr. Anup Chandra, Head of the Forest Botany Division at the Forest Research Institute, Dehradun, Uttarakhand. The authenticity of the plant material was confirmed by the Herbarium at the Forest Research Institute (FRI), and a voucher specimen was deposited under the number 1184/Dis/2018/Sys Bot/Rev Gen/4–5. Healthy leaves of *P. capitata* were collected and washed thoroughly with tap water to remove any dust particles. Following the cleaning, the leaves were air-dried for 15 to 20 days. The dried leaves were then pulverized into a fine powder using a mortar and pestle, and the resulting powder was stored in an airtight container at room temperature for later use.

Preparation of leaves extract

To get rid of any remaining dirt, fresh, healthy *P. capitata* leaves were properly cleansed in double-distilled water. The leaves had dried in the shade for fifteen days until they attained their steady weight. After crushing the dried leaves using a crusher and pestle, 10 g of *P. capitata* was added to 500 ml of double-distilled water in a 500 ml Erlenmeyer conical flask and heated to 70°C for 20 minutes. Following a period of cooling to room temperature, the extract (Fig. 1) was filtered using Whatman filter paper no. 1 in a separate conical flask.

Synthesis of gold nanoparticles using plant extract

P. capitata leaves, both fresh and dried, were repeatedly cleaned with deionized water. To obtain the extract, 10 g of chopped *P. capitata* leaves were cooked in 500 ml of deionized water and then filtered. For upcoming tests, the extract was filtered and kept at 4° C. The extract serves as a stabilizing and reducing agent. The Uttarakhand Educational Material Center provided the gold tetra chloroauric acid trihydrate ($HAuCl_4.3H_2O$), which was used without additional purification. All of the studies were conducted using de-ionized water. In order to create gold nanoparticles, aliquot amounts of *P. capitata* extract and gold chloroauric acid trihydrate were mixed with water. In a 2 L Erlenmeyer flask, 1 mM aqueous $HAuCl_4.3H_2O$ solution and *P. capitata* leaf extract were mixed in a 1:8 ratio. It was stored in a dark environment for seventy-two hours. The ocular hue changes from light yellow to stable violet in ten minutes, indicating rapid decline. After centrifuging the mixture for 20 minutes at 7500 rpm to remove contaminants, it was washed with distilled water and acetone and it was then dried at 50°C for 20 hours in an oven in order to characterize the gold nanoparticles and their anti-cancer activities. The final substance was crushed up in a mortar and pestle to create finely powdered golden blackish color nanoparticles. Figure 2 shows the general synthesis and characterization of nanoparticles using P. *capitata* extract.

Characterization

Using a Varian, Cary 100 UV-Vis spectrophotometer, the UV-vis spectra of the solution in quartz cuvettes were measured in the 200–800 range to track the bioreduction of the AuCl4-ions in solution. With the aid of the pictures captured by a Philips CM30 transmission electron microscope, the shape of the nanoparticles was examined. A MIRA3-LMU FE-SEM apparatus fitted with a Thermo EDAX attachment was used to characterize the gold nanoparticles in order to conduct the energy dispersive X-ray analysis (EDAX). Using KBr pellets as the sample, the FT-IR spectra were acquired using a Bruker FTIR instrument type Tensor 27. An X'Pert-Pro diffractometer made by PAN analytical was used to acquire the X-ray diffraction pattern of dry nanoparticle powder using monochromatized Cu Kα radiation (l = 1.54 Å).

Anticancer activity and antimicrobial activity procedures

Female Swiss albino mice aged 12 weeks weighing 20–25 g were obtained from the animal facility of NCS LAB Research and Development Centre Nagpur Maharashtra India. The animals were housed and handled in accordance with CPCSEA guidelines, and all experimental procedures were conducted following approval from the Institutional Animal Ethics Committee of NCS LAB R&D Centre. The mice were acclimatized for 7 days (Days 1–7), during which their health and body weight were monitored daily. They were then randomly assigned to three groups: Group 1 (negative control: sterile saline vehicle only), Group 2 (positive control: cyclophosphamide monohydrate at 5 µg/mL), and Group 3 (test group: P. capitata-AuNPs at 20 µg/mL).

Tumors were induced by subcutaneously injecting 1×10^6 viable Hep-2 cells (suspended in 100–200 µL PBS/Matrigel mix) into the right flank of each mouse. Anesthesia was administered using Propofol at

10–20 mg/kg body weight (1–2% concentration, 10–20 mg/mL), via intraperitoneal (IP) or intravenous (IV) routes, with a duration of 10–30 minutes before injection. Tumor formation was confirmed by palpation, with tumors reaching a maximum volume of 1000 mm^3 by Days 10–14 (initial volume: 0.42 ± 0.25 cm^3).

From Days 8–28 (approximately 3 weeks), treatments were administered intraperitoneally (IP) or orally (PO) once daily for 21 days, with doses calculated based on body weight. Group 1 received 100–200 µL sterile saline, Group 2 received 100–200 µL cyclophosphamide solution (5 µg/mL in saline), and Group 3 received 100–200 µL AuNP suspension (20 µg/mL in saline, sonicated for uniformity). Mice were monitored daily for body weight, tumor size (measured with calipers; volume = (length × $width^2$)/2), behavior, and toxicity signs (e.g., lethargy or ≥ 20% weight loss). Any mouse with tumor volume exceeding 2000 mm^3 or meeting humane endpoints was euthanized.

On Day 29, all remaining mice were humanely euthanized via CO_2 asphyxiation following anesthesia with isoflurane (5% dosage, 5% concentration in oxygen, inhalation route, 5–10 minutes duration). Blood samples were collected into EDTA tubes for hematological analysis, and tumors were excised from the flank, weighed immediately (mean weight: 1.56 ± 0.82 g), homogenized on ice, and centrifuged (5000 rpm, 10 min, 4°C) for cell suspension viability assessment. From Days 29–32, hematological parameters (RBC, WBC, and Hb) were evaluated to assess treatment effects.

The Hep-2 cell line was obtained from NCS LAB Research and Development Centre Nagpur Maharashtra India and used for tumor induction experiments.

In-vitro Anti-microbial Activity activities

In this study for antibacterial test the following species such as *Bacillus subtilis, Escherichia coli*, and *Aspergillus oryzae* were obtained from NCS LAB R&D, Nagpur, Maharashtra, India. For evaluate the antifungal potential of biosynthesized AuNPs from *P. capitata*, adapt the disk diffusion procedure for yeast strains such as *Candida albicans* (ATCC 10231), following CLSI M44-A2 guidelines for antifungal susceptibility testing. Prepare Sabouraud dextrose agar (SDA) plates by pouring 20 mL molten media into sterile Petri dishes and allowing solidification. Standardize the fungal inoculum to 0.5 McFarland turbidity (~ 1–5 × 10^6 CFU/mL) using yeast suspension in sterile saline, verified by OD530 ~ 0.08–0.10. Inoculate SDA plates with 100 µL inoculum via sterile swab for uniform lawn formation. Apply disks impregnated with 10 µL AuNP suspension (100 µg/mL, ~ 1 µg AuNPs/disk), fluconazole (25 µg/disk as positive control), and saline (negative control), ensuring 20 mm spacing. Incubate inverted plates at 35°C for 24–48 hours. Measure inhibition zones post-incubation: expected AuNP zones of 8–12 mm against *C. albicans* indicate moderate activity (~ 30–40% of fluconazole's 25–30 mm zone), attributed to AuNP-induced ROS-mediated membrane damage, ergosterol disruption, and synergistic phytochemical effects from *P. capitata* extracts enhancing fungal cell wall penetration. Negative controls show no zones, while statistical analysis (ANOVA, $p < 0.05$) confirms significance; this highlights AuNPs' promise as broad-

spectrum antifungals, warranting further MIC testing and biofilm disruption assays for clinical pathogens like azole-resistant *C. albicans* strains.

Statically analysis

Origin 8 software was utilized to evaluate variance using a one-way ANOVA. The standard deviation (SD) and average of the three runs of each measurement, which were performed three times (n = 3), are displayed. Significance was determined using $P \leq 0.05$.

Results and Discussion

Synthesis of gold nanoparicles using plant extract is useful not only because of its reduced environmental, but also because it can be used to produce large quaniies of nanoparicles. Plant extracts may act both as reducing agents and stabilizing agents in the synthesis of nanoparicles [40]. In view of its simplicity, the use of plant extract for reducing metal salts to nanoparicles has atracted considerable atenion within the last few decades [15]. The properies of gold nanoparicles are very diferent from that of bulk, as the gold nanoparicles are wine red soluion while the bulk gold is yellow solid. The gold nanoparicles can be manufactured into a variety of shapes including nanorods, nanospheres, nanocages, nanostars, nanobelts and nanoprisms [41]. The size and shape of gold nanoparicles strongly inluence their chemical and other properies. The triangular shaped nanoparicles show atracive opical properies in comparison to spherical one [42]. Due to their wide spread applicaions in targeted drug delivery, imaging, diagnosis and therapeuics due to their extremely small size, high surface area, stability, non-cytotoxicity and tunable opical, physical and chemical properies, gold nanoparicles have revoluionised the ield of medicine [41, 43].

From the previous result, the aqueous extract of *P. capitata* leaves contains important bioactive compounds such as saponins, phenolic compounds, tannins, flavonoids, alkaloids, steroids, and glucosides which are responsible for gold nanoparticle preparation [44]. These phytochemicals possess *P. capitata* to have different pharmaceutical activities such as antibacterial, antioxidant, lipid peroxidation, metal ion reduction and stabilization abilities [45]. In this study, phytochemicals obtained from aqueous leaf extract of *P. capitata* was utilized to cap Au^{3+} ions, thereby promoting the nucleation of the mixture into AuNPs, along with their subsequent stabilization. The synthesized AuNPs were then characterized employing various analytical techniques and evaluated for their potential photocatalytic, antioxidant, and antibacterial activities. Figure 4 showed some important bioactive compounds such as quercetin kaempferol, taxifolin, gallic acid, vanillic acid and protocatechuic acid important for gold nanoparticle synthesis [46].

UV-Visible Analysis

The appearance of a purple color following mixing of the plant extract with $HAuCl_4$ solution indicated the formation of AuNPs[47]. Using UV-vis spectroscopy, the resultant colloidal solutions were investigated. Typical spectra obtained with AuNPs are shown in Fig. 5. It is evident that the AuNP-absorption peaks in three of the spectra appeared at wavelengths between 520 and 550 nm. In this study, a rapid and eco-friendly biosynthesis of AuNPs using leaf extract of *P. capitata* was synthesized. Remarkably, the formation of AuNPs was completed within just five minutes without the need for external stimuli such as heating, stirring, or pH adjustments, highlighting the efficiency and simplicity of this green synthesis approach. The bioactive compounds (Fig. 5) present in the *P. capitata* leaf extract not only facilitated the reduction of gold ions (Au^{3+}) to elemental gold but also acted as natural capping agents, stabilizing the nanoparticles. Optimal synthesis was achieved at a volume ratio of 1:8 (100 mL leaf extract to 800 mL auric chloride solution), ensuring maximum yield and stability. The successful formation of AuNPs was visually confirmed by a distinct color change of the solution from light pink to a deep pinkish-purple hue (Fig. 5), a hallmark of nanoparticle surface plasmon resonance.

UV-Vis spectroscopic analysis revealed a broad absorption peak cantered at 534 nm, indicative of the characteristic surface plasmon resonance of gold nanoparticles[48]. This peak corresponds to an estimated energy band gap of 2.32 eV, consistent with the quantum confinement effects observed in nanoscale gold particles. These findings align well with previous reports where biosynthesized gold nanoparticles exhibited absorption peaks typically ranging from 520 to 550 nm, depending on particle size and shape[49]. For instance, gold nanoparticles synthesized using *Azadirachta indica* leaf extract showed an absorption maximum around 535 nm with a band gap close to 2.3 eV, underscoring the comparable optoelectronic properties achieved through different green synthesis routes[50].

XRD analysis

The structure of the gold nanoparticles that were created from the material was examined using XRD (Fig. 6). The angular orientations of the Bragg peaks were used to determine the cubic close packed (ccp) phase crystalline nature form of the gold nanoparticles. The XRD spectrum demonstrated the crystalline structure of the gold nanoparticles. Sharp peaks were seen in the XRD spectra of the produced nanoparticles at $2\theta = 38.25°$, 44.46^{o}, and 64.70^{o} in that order. These peaks line up with the cubic closed packed phase nano crystals lattice planes (111), (200) and (220)[51].

TEM analysis

The surface morphology of gold nanostructures was investigated using TEM examination (Fig. 7). These findings confirmed the spherical and triangular shape and less than 15 nm average size of the gold nanoparticles. The main method for creating metal nanoparticles is to use lethal reducing agents. A number of biomimetic techniques are being researched to produce biocompatible nanoparticles. The astonishing discoveries being made in the realm of nanoparticle application in medicine are certainly supported by the growing body of research in this area. This calls for the usage of nanoparticles that are safe for biological systems. By prioritizing the production of environmentally sustainable nanoparticles,

biological technologies might present a viable substitute for conventional methods. However, limitations like pH shift and incubation are the result of large scale manufacture. Greener methods of producing nanoparticles show promise in circumventing the issues associated with microbial nanoparticle manufacturing. This study uses an extract from the leaves of the medicinal plant Persicaria capitata to investigate the biological synthesis of gold nanoparticles.

A comparable size of nanoparticle was obtained by [52] using leaf extract of *Cacumen platyclade* having a size of 15.3 nm. Their result indicated that, the synthesized NPs were of diverse morphology such as sphere, triangles. In this synthesis flavonoids and reducing sugars act both as reducing and protecting agent. Au NPs has also been synthesized using *Cerasus serrulata* leaf extract [53]. The synthesized NPs has size in range from 5 to 25 nm and spherical in shape. *C. serrulata* contain was obtained. Au NPs have also been synthesized using root extract of *Morinda citrifolia*. A higher AuNPs size was obtained by [54], their result indicated that AuNPs with nanoparticle size of 38 − 26 nm was obtained using root extract of *Morinda citrifolia*.

EDX analysis

The composition of the synthesized gold nanoparticles (AuNPs) was analyzed using Energy Dispersive X-ray Spectroscopy (EDX) (Fig. 8). A distinct and sharp signal at approximately 2.1 keV confirmed the presence of elemental gold, consistent with the characteristic X-ray emission of Au. Additionally, a modest peak observed around 0.5 keV corresponded to oxygen, which is likely attributed to biomolecules or organic compounds adsorbed on the surface of the AuNPs. These biomolecules, derived from the plant extract, may act as capping and stabilizing agents, preventing nanoparticle aggregation and enhancing biocompatibility. Furthermore, the presence of other minor signals in the EDX spectra could be indicative of trace elements or bioactive substances inherent to the *P. capitata* leaf extract, which may contribute to the reduction and stabilization processes during nanoparticle synthesis. This elemental analysis supports the successful green synthesis of AuNPs with surface functionalization by phytochemicals, which could influence their physicochemical properties and potential biomedical applications.

FTIR Analysis

It was possible to identify putative biomolecule functional groups that could have helped produce Au nanoparticles by using Fourier transform infrared (FTIR) spectrum analysis. The O-H stretch, C-H stretch in aromatic ring & Isocyanate stretch are the regions of the FTIR spectrum that displayed absorption peaks at 3377, 2924 and 2345 cm^{-1}. [55–57]

Fourier Transform Infrared (FTIR) spectroscopy (Fig. 9) was employed to identify putative biomolecular functional groups that may have contributed to the synthesis and stabilization of the gold nanoparticles (AuNPs). The FTIR spectrum exhibited several characteristic absorption peaks, including a broad O–H stretching vibration at 3377 cm-1, indicative of hydroxyl groups commonly found in alcohols and phenolic compounds[58]. A peak at 2924 cm-1 corresponded to C–H stretching vibrations in aromatic

rings or aliphatic chains[59]. The absorption band at 2345 cm-1 was assigned to the isocyanate (–N = C = O) stretch, which may arise from specific biomolecules in the plant extract[60]. Additional peaks were observed at 1635 cm-1, corresponding to the C = O stretching vibration of amide I groups or conjugated carbonyls, suggesting the presence of proteins or polyphenols [60]. The band near 1384 cm-1 was attributed to C–H bending vibrations, while the peak at 1045 cm-1 indicated C–O stretching vibrations, typical of alcohols, ethers, or polysaccharides.[61] These functional groups are likely involved in the reduction of Au^{+3} ions to Au and act as capping agents, stabilizing the nanoparticles by preventing aggregation. The FTIR analysis thus confirms the role of diverse phytochemicals in the biological synthesis and surface functionalization of AuNPs.

In-vitro Anti-cancer activity

In cytotoxicity assays of the nanoparticles against the Hep-2 cell line, 50% cytotoxicity (IC50) was observed at 20 µg/ml. In comparison, the standard drug cyclophosphamide monohydrate showed 50% cytotoxicity at 5 µg/ml against the same cell line. The IC50 values were 20 µg/ml for *P. capitata* gold nanoparticles and 5 µg/ml for cyclophosphamide monohydrate. No cytotoxicity was observed with DMSO (negative control). The results are summarized in Table 2. Before the anticancer experiment, the cell concentration (number of cells) in both cancer cell lines was increased. The Hep-2 cell line was treated with 40 µg/ml of nanoparticles and analyzed using MTT and Sulforhodamine B (SRB) assays. Both assays demonstrated that *P. capitata* gold nanoparticles were effective against the Hep-2 cell line, and the results from the two methods were consistent.

Using the SRB assay, *P. capitata* gold nanoparticles (20 µg/ml) reduced Hep-2 cancer cell viability by 64.32%. In contrast, the positive control, cyclophosphamide monohydrate (5 µg/ml), showed 85.0% inhibition of cancer cells (Table 1). Similarly, the MTT assay showed that *P. capitata* gold nanoparticles (20 µg/ml) inhibited Hep-2 cancer cells by 68.45%, while cyclophosphamide monohydrate (5 µg/ml) showed 82.23% inhibition .

The Table 2 provides important information on the viability and condition of the Liver (Hep-2) cell line prior to the anticancer assay, assessed using the Trypan blue exclusion method (Fig. 10). The cells exhibit a high viability of 80.02%, indicating that the majority of the cell population is alive and healthy, which is crucial for reliable experimental outcomes. The live cell count of 1.23 × 10^6 cells, compared to a total cell count of 2.18 × 10^6 cells, further supports this viability percentage. Additionally, the culture medium's pH of 7.4 falls within the optimal physiological range, ensuring a suitable environment for cell growth and function. Together, these parameters confirm that the Hep-2 cells are in good condition and appropriately prepared for subsequent anticancer testing, thereby reducing the risk of confounding effects due to poor cell health or unfavorable culture conditions.

Table 1
Percent cell viability and characterization of cell lines via Trypan blue assay (before anticancer assay)

Cell lines	Percent viability	Live cell count	Total cell count	pH
Liver (Hep-2)	80.02%	$1.23x10^6$	$2.18x10^6$	7.4

The Table 2 presents the cytotoxic effects of various samples on the Liver (Hep-2) cancer cell line by reporting their IC50 values, which represent the concentration needed to inhibit 50% of the cancer cells. Cyclophosphamide monohydrate, a well-known chemotherapeutic drug, exhibits the lowest IC50 value of 5.0 µg/ml, indicating its strong potency against Hep-2 cells. In comparison, gold nanoparticles synthesized from *P. capitata* show a higher IC50 value of 20.0 µg/ml, reflecting moderate cytotoxic activity and suggesting their potential as an anticancer agent, though less effective than cyclophosphamide. The solvent control, DMSO, shows no cytotoxicity with an IC50 value of 0.0 µg/ml, confirming its inert nature in this assay. Overall, these findings highlight the superior efficacy of cyclophosphamide while indicating that the gold nanoparticles possess promising anticancer properties that may benefit from further refinement to improve their therapeutic potential.

Table 2
Cytotoxicity assay of nanoparticles against Hepatic (Hep-2) cancer cell line (IC50 values determination)

Samples	**IC50 values (µg/ml)**
	Cancer cell lines used
	Liver (Hep-2)
Cyclophosphamide monohydrate	5.0
Gold nanoparticle of Persicaria capitata	20.0
DMSO	0.0

Table 3 presents the results of the Sulforhodamine B (SRB) assay, which measures the percent inhibition of cancer cell growth in the Hepatic (Hep-2) cell line after treatment with two different samples: gold nanoparticles of *P. capitata* at 20 µg/ml and cyclophosphamide monohydrate at 5 µg/ml. The data show that cyclophosphamide monohydrate achieves a higher percent inhibition of 85.0%, indicating strong anticancer activity and effective suppression of Hep-2 cell proliferation. In comparison, the gold nanoparticles of *P. capitata* exhibit a lower but still significant inhibition of 64.32%, demonstrating moderate anticancer potential. These results align with previous cytotoxicity findings, confirming that while cyclophosphamide remains more potent, the gold nanoparticles also possess notable anticancer effects and could be considered for further development as therapeutic agents.

Table 3
Sulphorodamine assay in hepatic (hep-2) cell line

	Percent inhibition of cancer cells	
Sulphorodamine B assay **In hepatic (hep-2) cell line**	**Gold nanoparticle of** **Persicaria capitata (20µg/ml)**	**Cyclophosphamide monohydrate (5 µg/ml)**
	64.32	85.0

The Table 4 displays the results of the MTT assay, which evaluates the percent inhibition of cancer cell growth in the Hepatic (Hep-2) cell line following treatment with gold nanoparticles of *P. capitata* (20 µg/ml) and cyclophosphamide monohydrate (5 µg/ml). The data indicate that cyclophosphamide monohydrate achieves a higher inhibition rate of 82.23%, reflecting its strong cytotoxic effect and effectiveness in reducing Hep-2 cell viability. Meanwhile, the gold nanoparticles show a substantial but comparatively lower inhibition of 68.45%, suggesting moderate anticancer activity. These findings are consistent with other assays, reinforcing that while cyclophosphamide remains the more potent agent, the gold nanoparticles possess significant anticancer properties and hold promise for further investigation as potential therapeutic agents.

Table 4
MTT assay in hepatic (hep-2) cell line

	Percent inhibition of cancer cells	
MTT assay in hepatic (hep-2) cell line	**Gold nanoparticles of P. capitata (20µg/ml)**	**Cyclophosphamide monohydrate (5 µg/ml)**
	68.45	82.23

In-vivo Anti-cancer activity

The data presented in Table 5 illustrate the effects of different treatments on various hematological and tumor-related parameters in animal models used for evaluating anticancer activity.

The 1st Group, serving as the negative control, shows the highest tumor weight (1.56 ± 0.82 g) and viable cell count (4.23 ± 0.45 × 10^6 cells/ml), indicating active tumor growth and cell viability without any treatment. The non-viable cell count is low (0.32 ± 0.75 × 10^6 cells/ml), consistent with minimal tumor cell death. Additionally, this group has relatively higher RBC (7.23 ± 0.92 × 10^6 cells/ml), WBC (7.56 ± 0.85 × 10^6 cells/ml), and hemoglobin levels (12.23 ± 0.62 g/dl), reflecting normal hematological status in untreated animals. In contrast, the 2nd Group, the positive control, shows a significant reduction in tumor weight (0.52 ± 0.53 g) and viable cell count (2.56 ± 0.48 × 10^6 cells/ml), indicating effective tumor suppression by the standard anticancer treatment. The non-viable cell count increases (0.67 ± 0.53 × 10^6 cells/ml), suggesting enhanced tumor cell death. However, this group also exhibits decreased RBC (4.54 ± 0.75 × 10^6 cells/ml), WBC (5.57 ± 0.64 × 10^6 cells/ml), and hemoglobin (8.37 ± 0.48 g/dl), which

may reflect some hematological toxicity or side effects associated with the treatment. The 3rd Group, treated with Test-B, demonstrates the lowest tumor weight (0.42 ± 0.25 g) and viable cell count (1.78 ± 0.25 × 10^6 cells/ml), indicating a strong anticancer effect, potentially superior to the positive control. The non-viable cell count is markedly higher (1.85 ± 0.25 × 10^6 cells/ml), suggesting increased tumor cell apoptosis or necrosis. Interestingly, RBC (5.23 ± 0.23 × 10^6 cells/ml), WBC (7.12 ± 0.25 × 10^6 cells/ml), and hemoglobin (12.02 ± 0 g/dl) levels are better maintained compared to the positive control, indicating that Test-B may exert less hematological toxicity while effectively reducing tumor burden.

This study examined the in vivo anticancer activity of gold *P. capitata* nanoparticles (20 µg/ml) using human cancer cell lines, namely liver (hep-2). Numerous parameters, such as tumor mass, Hemoglobin content, viable and non-viable cell counts, and the counts of red and white blood cells were also evaluated as part of the anticancer research. The results of the present investigation suggest that the nanoparticles were effective in lowering the quantity of cancer cells in the Swiss albino mice's livers. To compare the study results, cyclophosphamide monohydrate (5 µg/ml) was employed as a positive control. The hepatic cells involved in the growth of tumors were further homogenized from animals (different groups: positive control, negative control, and treated), as the study examined. The tumor weight of the first group (negative control) of hepatic (hep-2) cancer cell line negative control groups was determined to be 1.56 g. The second group's tumor mass was found to be 0.52 g, while the third group's tumor mass was 0.42 g.

Table 5
Parameters determined in different sets of animal models for evaluation of anticancer activity

Groups	**Parameters evaluated**					
	Tumor weight (g)	Viable cell count (cellsx10^6/ml)	Non-viable cell count (cellsx10^6/ml)	RBC (cellsx10^6 /ml)	WBC (cellsx10^6 /ml)	Hemoglobin (g/dl)
1st Group- Negative Control	1.56 ± 0.82	4.23 ± 0.45	0.32 ± 0.75	7.23 ± 0.92	7.56 ± 0.85	12.23 ± 0.62
2nd Group- Positive Control	0.52 ± 0.53	2.56 ± 0.48	0.67 ± 0.53	4.54 ± 0.75	5.57 ± 0.64	8.37 ± 0.48
3th Group- Test-B	0.42 ± 0.25	1.78 ± 0.25	1.85 ± 0.25	5.23 ± 0.23	7.12 ± 0.25	12.02 ± 0

Where: 1st Group- Negative Control - Mice administered with Hepatic (Hep-2) cancer cell lines only; 2nd Group- Positive Control- Mice administered with Hep-2 cancer cell lines injected with Cyclophosphamide

monohydrate (5 µg/ml); 3th Group- Test-B- Mice administered with Hepatic (Hep-2) cancer cell lines injected with gold nanoparticles of *P. capitata* (20 µg/ml).

In-vitro Anti-microbial Activity

To evaluate the antimicrobial potential of the synthesized nanoparticles, assays were conducted against two bacterial strains (*Bacillus subtilis* and *Escherichia coli*) (Fig. 11) and two fungal strains (*Candida albicans* and *Aspergillus oryzae*) as shown in Fig. 12. Standard antibiotics, azithromycin (for bacteria) and fluconazole (for fungi), were used as positive controls and exhibited clear zones of inhibition. Gold nanoparticles synthesized using the leaf extract of *P. capitata* showed antibacterial activity, with inhibition zones ranging from 7.0 mm for *Bacillus subtilis* to 10.0 mm for *E. coli*. Similarly, AuNPs synthesized from *Pyracantha crenulata* leaf extract demonstrated antifungal activity, with inhibition zones of 15.0 mm for *Candida albicans* and 10.0 mm for *Aspergillus oryzae*. Clear zones of inhibition confirmed the antimicrobial potential of the biosynthesized nanoparticles.

Table 6 evaluates the antimicrobial activity of gold nanoparticles (AuNPs) synthesized from *P. capitata* extract against *Bacillus subtilis* (Gram-positive) and *Escherichia coli* (Gram-negative) using the disk diffusion method at 100 µg/ml, with Azithromycin as the positive control. The AuNPs produced zones of inhibition of 7.0 mm against *B. subtilis* and 10.0 mm against *E. coli*, indicating moderate antibacterial effects with slightly better efficacy toward the Gram-negative strain, possibly due to enhanced penetration of the thinner peptidoglycan layer or outer membrane disruption facilitated by phytochemicals like flavonoids in the plant extract. In comparison, Azithromycin generated larger zones of 25.0 mm and 28.0 mm, respectively, reflecting its strong, broad-spectrum potency via inhibition of bacterial protein synthesis, aligning with CLSI susceptibility standards (> 21 mm). The AuNPs' activity represents about 28–36% of the antibiotic's efficacy, highlighting inherent nanoparticle mechanisms such as reactive oxygen species generation or membrane damage, though limited by factors like bacterial cell wall thickness—thicker in Gram-positive *B. subtilis*—and assay variables including diffusion rates and incubation conditions (24–48 hours at 37°C). Zones under 10 mm typically denote moderate activity, positioning AuNPs as promising but not superior to conventional antibiotics.

These findings suggest green-synthesized AuNPs from *P. capitata* as eco-friendly adjuncts or alternatives for tackling antibiotic-resistant infections, particularly Gram-negative ones like *E. coli*, amid rising antimicrobial resistance. However, limitations include testing only two strains at a single concentration, necessitating broader evaluations against clinical isolates, fungi, or biofilms, alongside quantitative MIC assays and mammalian cell toxicity profiles for biocompatibility. Phytochemical analysis could further clarify the extract's role in boosting AuNP stability and bioactivity. Optimization strategies, such as increasing concentrations, reducing particle size, or combining with antibiotics, may enhance potency. Table 6 underscores the potential of biosynthesized nanomaterials in sustainable antimicrobial research, though further mechanistic studies are essential for practical applications.

Table 6
Antimicrobial activity of gold nanoparticles against different bacterial strains.

S. No.	Samples (100 µg/ml)	Diameter of zone of inhibition (mm)/Antimicrobial activity	
1.		*Bacillus subtilis*	*E. coli*
2.	Gold nanoparticles of *Persicaria capitata*	7.0	10.0
3.	Azithromycin	25.0	28.0

Table 7
Antimicrobial activity of gold nanoparticles against different fungal strains.

S. No.	Samples (100 µg/ml)	Diameter of zone of inhibition (mm)/Antimicrobial activity	
1.		*Aspergillus oryzae*	*Candida albicans*
2.	Gold nanoparticles of *P. capitata*	10.0	15.0
3.	Fluconazole	18.0	28.0

Conclusion

We successfully developed a green route for the synthesis of colloidal AuNPs using the aqueous leaf extract of *P. capitata* as a renewable bioresource. The nanoparticles were characterized by UV–Vis, TEM, XRD, EDX, and FTIR, revealing predominantly spherical particles with an average size of ~ 15 nm. Reaction parameters such as temperature, contact time, and pH influenced nanoparticle morphology. The synthesized AuNPs demonstrated significant antimicrobial and anticancer activities, with cytotoxicity assays confirming dose-dependent inhibition of hepatic (Hep-2) cancer cells. These findings suggest that *P. capitata*-derived AuNPs hold promise as sustainable nanomaterials for biomedical applications. Future studies should focus on elucidating their mechanisms of action, in vivo safety, and clinical validation.

Declarations

Acknowledgements

The authors are grateful to USIC, HNB Garhwal University and Punjab University, Chandigarh for supplying the XRD, UV- Visible spectrophotometer, TEM and EDX results and the anticancer activity done by the internal institutional ethical committee [NCS/R&D/230101] NCS Group, Nagpur, Maharashtra, India and the funds for this work were provided by UCOST Dehradun (Project no. UCS&T/R&D-28/20-21/19944/1) for which I am very thankful to them.

Author contributions

Limenew Abate Worku, Stuti Gupta, M.C. Purohit, Reena Purohit, Shikha Syal1, and Sonali Purohit contributed to the first draft of the paper. Stuti Gupta, Anuj Kandwa, Archana Bachheti, and Rakesh Kumar Bachhet handled data collecting and material preparation., Stuti Gupta, M.C. Purohit, Reena Purohit, Shikha Syal1, Sonali Purohit, Anuj Kandwal material preparation. Limenew Abate Worku analysis the data and supervise the research work. Every contributor contributed to the article's revision as well.

Funding: No funding

Competing interests

The authors declare no competing interests.

Ethics and consent to participate

Leaves of *Persicaria capitata* were collected from non-protected, non-private, and non-indigenous land located in the Nagdev Forest range, Pauri, Uttarakhand, India. The collection complied with applicable local and national guidelines for plant material collection. Prior informed consent was obtained from relevant stakeholders, The plant was taxonomically identified by Dr. Anup Chandra, Head, Forest Botany Division, Forest Research Institute, Dehradun, and a voucher specimen was deposited at the FRI Herbarium (Voucher No. 1184/Dis/2018/Sys Bot/Rev Gen/4-5). Ethical approval for the in vivo experiments was obtained from the Institutional Animal Ethics Committee of NCS LAB Research and Development Centre NCS Group Nagpur Maharashtra India Approval No NCS R&D 230101. All experimental animals were owned and maintained by NCS LAB Research and Development Centre Nagpur Maharashtra India and informed institutional permission was obtained prior to their use in the study.

Data availability

Data is provided within the manuscript

Consent to publish

Not applicable

References

1. Murphy CJ et al (2005) Anisotropic metal nanoparticles: synthesis, assembly, and optical applications. J Phys Chem B 109:13857–13870
2. Sun Y et al (2017) Temperature-sensitive gold nanoparticle-coated pluronic-PLL nanoparticles for drug delivery and chemo-photothermal therapy. Theranostics 7:4424

3. Nguyen TT et al (2018) Iron oxide and gold based magneto-plasmonic nanostructures for medical applications: a review. Nanomaterials 8:149
4. Fazal S et al (2014) Green synthesis of anisotropic gold nanoparticles for photothermal therapy of cancer. ACS Appl Mater Interfaces 6:8080–8089
5. Wang C et al (2016) Characterization and antimicrobial application of biosynthesized gold and silver nanoparticles by using Microbacterium resistens. Artif Cells Nanomed Biotechnol 44:1714–1721
6. Khan M et al (2018) Green synthesis and characterization of silver nanoparticles using Coriandrum sativum leaf extract. J Eng Sci Technol 13:158–166
7. Veisi H et al (2018) Green synthesis of Au nanoparticles using an aqueous extract of Stachys lavandulifolia and their catalytic performance for alkyne/aldehyde/amine A3 coupling reactions. RSC Adv 8:38186–38195
8. Mukherjee S et al (2014) Potential theranostics application of bio-synthesized silver nanoparticles (4-in-1 system). Theranostics 4:316
9. Benedec D et al (2018) Origanum vulgare mediated green synthesis of biocompatible gold nanoparticles simultaneously possessing plasmonic, antioxidant and antimicrobial properties. Int J Nanomed 13:1041–1058
10. Francis S et al (2017) Green synthesis and characterization of gold and silver nanoparticles using Mussaenda glabrata leaf extract and their environmental applications to dye degradation. Environ Sci Pollut Res 24:17347–17357
11. Cruz DM et al (2019) Citric juice-mediated synthesis of tellurium nanoparticles with antimicrobial and anticancer properties. Green Chem 21:1982–1998
12. Mohammadinejad R et al (2019) Plant molecular farming: production of metallic nanoparticles and therapeutic proteins using green factories. Green Chem 21:1845–1865
13. Borase HP et al (2014) Plant extract: a promising biomatrix for ecofriendly, controlled synthesis of silver nanoparticles. Appl Biochem Biotechnol 173:1–29
14. Iravani S (2011) Green synthesis of metal nanoparticles using plants. Green Chem 13:2638–2650
15. Mittal AK et al (2013) Synthesis of metallic nanoparticles using plant extracts. Biotechnol Adv 31:346–356
16. Mirkin CA et al (2020) A DNA-based method for rationally assembling nanoparticles into macroscopic materials. Spherical Nucleic Acids. Jenny Stanford Publishing, pp 3–11
17. Sen IK et al (2013) Green synthesis of gold nanoparticles using a glucan of an edible mushroom and study of catalytic activity. Carbohydr Polym 91:518–528
18. Rao C et al (2001) Science and technology of nanomaterials: current status and future prospects. J Mater Chem 11:2887–2894
19. Crumbliss A et al (1992) Colloidal gold as a biocompatible immobilization matrix suitable for the fabrication of enzyme electrodes by electrodeposition. Biotechnol Bioeng 40:483–490

20. Sun Y et al (2002) Shape-controlled synthesis of gold and silver nanoparticles. Science 298:2176–2179
21. El-Sayed IH et al (2006) Selective laser photo-thermal therapy of epithelial carcinoma using anti-EGFR antibody conjugated gold nanoparticles. Cancer Lett 239:129–135
22. Wu W et al (2013) Two-step size-and shape-separation of biosynthesized gold nanoparticles. Sep Purif Technol 106:117–122
23. Huang X et al (2007) Gold nanoparticles: interesting optical properties and recent applications in cancer diagnostics and therapy. Nanomedicine 2:681–693
24. Hashmi ASK et al (2006) Gold Catal Angew Chem Int Ed 45:7896–7936
25. Alivisatos AP (1996) Perspectives on the physical chemistry of semiconductor nanocrystals. J Phys Chem 100:13226–13239
26. Jin R et al (2001) Photoinduced conversion of silver nanospheres to nanoprisms. Science 294:1901–1903
27. Aizpurua J et al (2003) Optical properties of gold nanorings. Phys Rev Lett 90:057401
28. Huang J et al (2007) Biosynthesis of silver and gold nanoparticles by novel sundried Cinnamomum camphora leaf. Nanotechnology 18:105104
29. Liao S-G et al (2011) Antibacterial and anti-inflammatory effects of extracts and fractions from Polygonum capitatum. J Ethnopharmacol 134:1006–1009
30. Alamgir A (2018) Secondary metabolites: secondary metabolic products consisting of C and H; C, H, and O; N, S, and P elements; and O/N heterocycles. In Therapeutic Use of Medicinal Plants and Their Extracts: Volume 2: Phytochemistry and Bioactive CompoundsSpringer, pp. 165–309
31. Petry C et al (2014) The propagation of Persicaria capitata in different substrates for green roof use. In XXIX International Horticultural Congress on Horticulture: Sustaining Lives, Livelihoods and Landscapes (IHC2014. V 1108:317–322
32. Mosissa D (2019) Invasive alien plant species in the northwestern & western provenance of Ethiopia and linking its' phonological implication to management and control
33. Bazzicalupo M (2021) Sustainable use of plants adapted to the Mediterranean climate as sources of bioactive compounds with health and environmental applications
34. Joshi M et al (1992) Response of water, temperature and light on germination behaviour of some successional species
35. Meier W (2006) Contribución al conocimiento de Persicaria nepalensis (Meisn.) H. Gross y P. capitata (Buch.-Ham. ex D. Don) H. Gross, especies invasoras en el Parque Nacional el Ávila, Venezuela. Acta Bot Venez 29:1–16
36. Berto R (2005) Exposure to restorative environments helps restore attentional capacity. J Environ Psychol 25:249–259
37. Cavanaugh LM (2008) Redefining the green roof. J Archit Eng 14:4–6
38. Simmonds N (1945) Polygonum persicaria L. J Ecol 33:121–131

39. Shahzadi S et al (2025) A review on green synthesis of silver nanoparticles (SNPs) using plant extracts: a multifaceted approach in photocatalysis, environmental remediation, and biomedicine. RSC Adv 15:3858–3903
40. Ikram S (2015) Synthesis of gold nanoparticles using plant extract: an overview. Nano Res 1:5
41. Thakor A et al (2011) Gold nanoparticles: a revival in precious metal administration to patients. Nano Lett 11:4029–4036
42. Ganeshkumar M et al (2012) Sun light mediated synthesis of gold nanoparticles as carrier for 6-mercaptopurine: preparation, characterization and toxicity studies in zebrafish embryo model. Mater Res Bull 47:2113–2119
43. Huang X et al (2010) Gold nanoparticles: optical properties and implementations in cancer diagnosis and photothermal therapy. J Adv Res 1:13–28
44. Nguyen V et al (2020) IOP Publishing,. Phytochemical screening, antioxidant activities, total phenolics and flavonoids content of leaves from Persicaria odorata Polygonaceae. In IOP Conference Series: Materials Science and Engineering Vol. 991, p. 012029
45. Seimandi G et al (2021) An update on phytochemicals and pharmacological activities of the genus Persicaria and Polygonum. Molecules 26:5956
46. He L et al (2025) A new phenolic compound from Persicaria capitata. Nat Prod Res 39:4097–4103
47. Husen A (2017) Gold nanoparticles from plant system: synthesis, characterization and their application. Nanoscience and Plant–Soil Systems. Springer, pp 455–479
48. Ghosh SK et al (2007) Interparticle coupling effect on the surface plasmon resonance of gold nanoparticles: from theory to applications. Chem Rev 107:4797–4862
49. Santhoshkumar J et al (2017) Phyto-assisted synthesis, characterization and applications of gold nanoparticles—a review. Biochem Biophys Rep 11:46–57
50. Gopalakrishnan V et al (2023) Enhanced antidiabetic and antioxidant properties of gold nanoparticles green synthesized using blossom extract of Azadirachta indica: in vitro studies. Inorg Chem Commun 158:111609
51. Krishnamurthy S et al (2014) Yucca-derived synthesis of gold nanomaterial and their catalytic potential. Nanoscale Res Lett 9:627
52. Zhan G et al (2011) Synthesis of gold nanoparticles by Cacumen Platycladi leaf extract and its simulated solution: toward the plant-mediated biosynthetic mechanism. J Nanopart Res 13:4957–4968
53. Karthik R et al (2016) Phyto mediated biogenic synthesis of gold nanoparticles using Cerasus serrulata and its utility in detecting hydrazine, microbial activity and DFT studies. J Colloid Interface Sci 468:163–175
54. Suman T et al (2014) The green synthesis of gold nanoparticles using an aqueous root extract of Morinda citrifolia L. Spectrochim. Acta Mol Biomol Spectrosc 118:11–16

55. Mudri NH et al (2020) Comparative study of aromatic and cycloaliphatic isocyanate effects on physico-chemical properties of bio-based polyurethane acrylate coatings. Polymers 12:1494
56. Zia KM et al (2014) Synthesis and molecular characterization of chitosan based polyurethane elastomers using aromatic diisocyanate. Int J Biol Macromol 66:26–32
57. Andrieu L et al (2025) Identification of polymeric binders in anticorrosive coatings via FTIR spectroscopy. Spectrochim Acta Mol Biomol Spectrosc. 126493
58. Ricci A et al (2015) Application of Fourier transform infrared (FTIR) spectroscopy in the characterization of tannins. Appl Spectrosc Rev 50:407–442
59. Liu J et al (2020) Three-step identification of infrared spectra of similar tree species to Pterocarpus santalinus covered with beeswax. J Mol Struct 1218:128484
60. Pasieczna-Patkowska S et al (2025) Application of Fourier transform infrared (FTIR) spectroscopy in characterization of green synthesized nanoparticles. Molecules 30:684
61. Thombare N et al (2023) Comparative FTIR characterization of various natural gums: a criterion for their identification. J Polym Environ 31:3372–3380

Figures

Figure 1

Plant extract of *P. capitata*

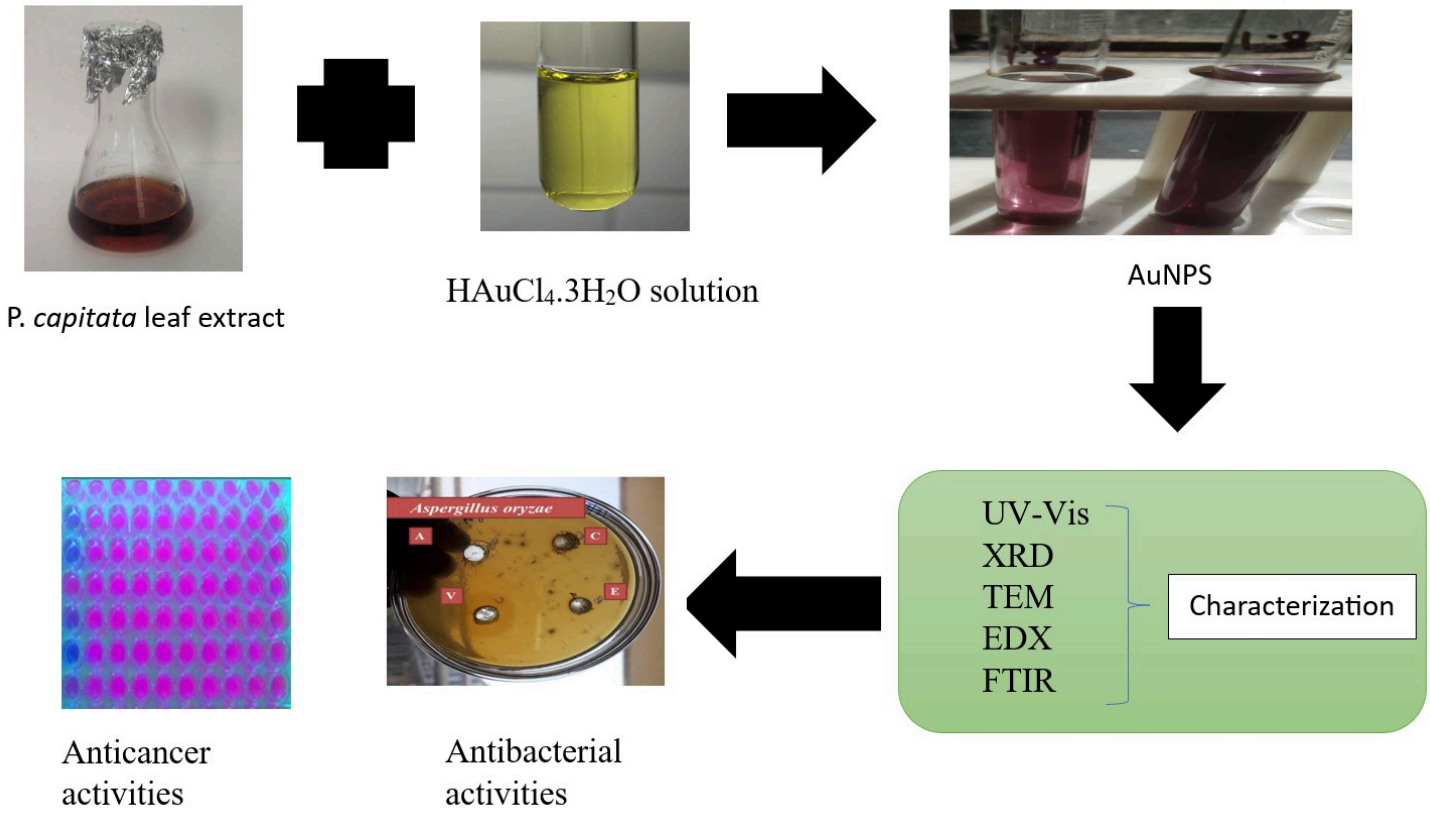

Figure 2

General method of synthesis and characterization of nanoparticles using plants

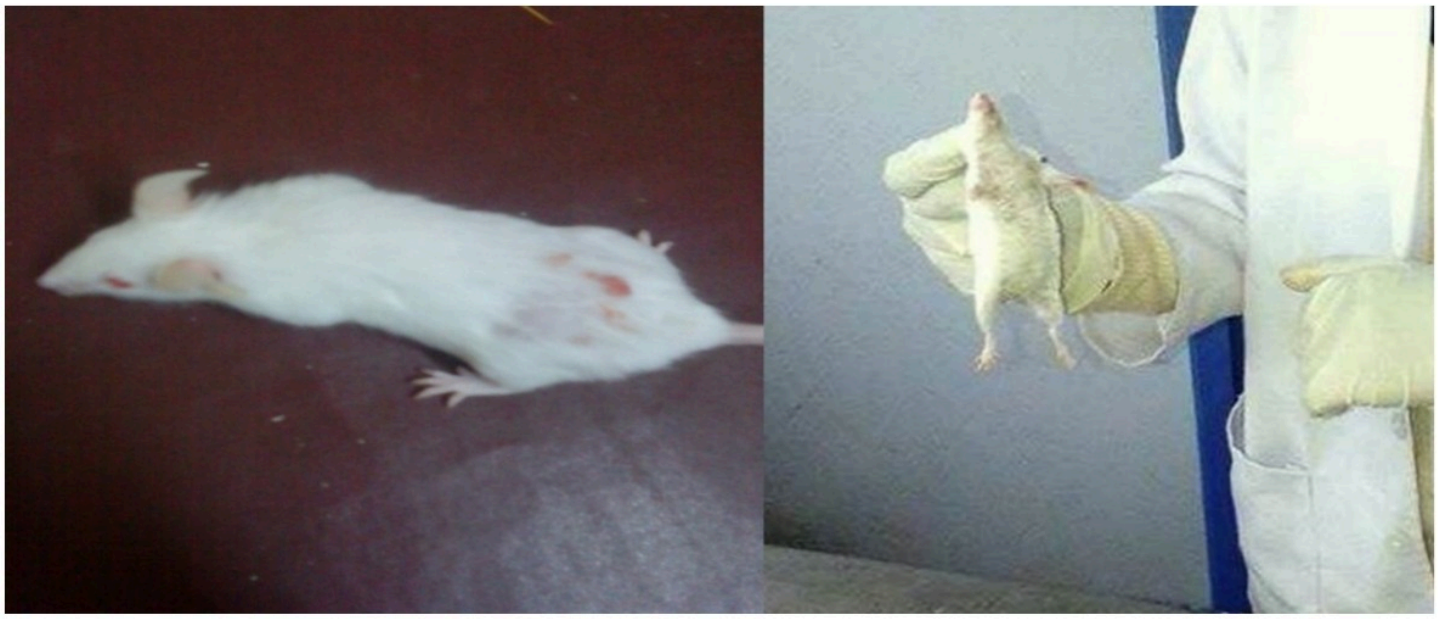

Figure 3

(**Left**) Cancer induction of cell line (hep-2) from NCS LAB R&D Nagpur Maharashtra in liver of Swiss albino rats. **(Right):**Dosing of nanoparticles via oral route.

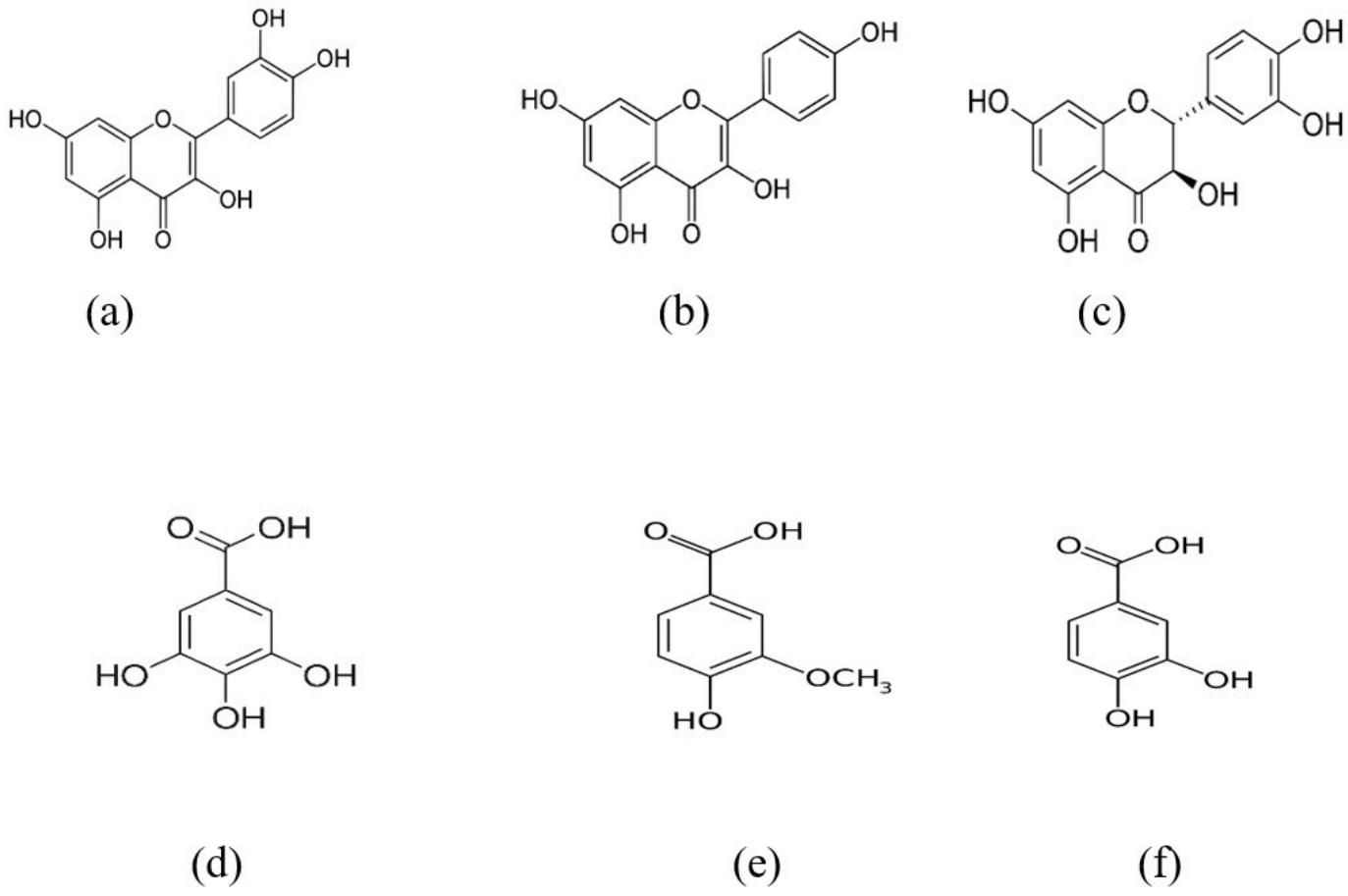

Figure 4

Structure of several compounds isolated from *P. capitata*: quercetin (a), kaempferol (b), taxifolin (c), gallic acid (d), vanillic acid (e), protocatechuic acid (f)[46].

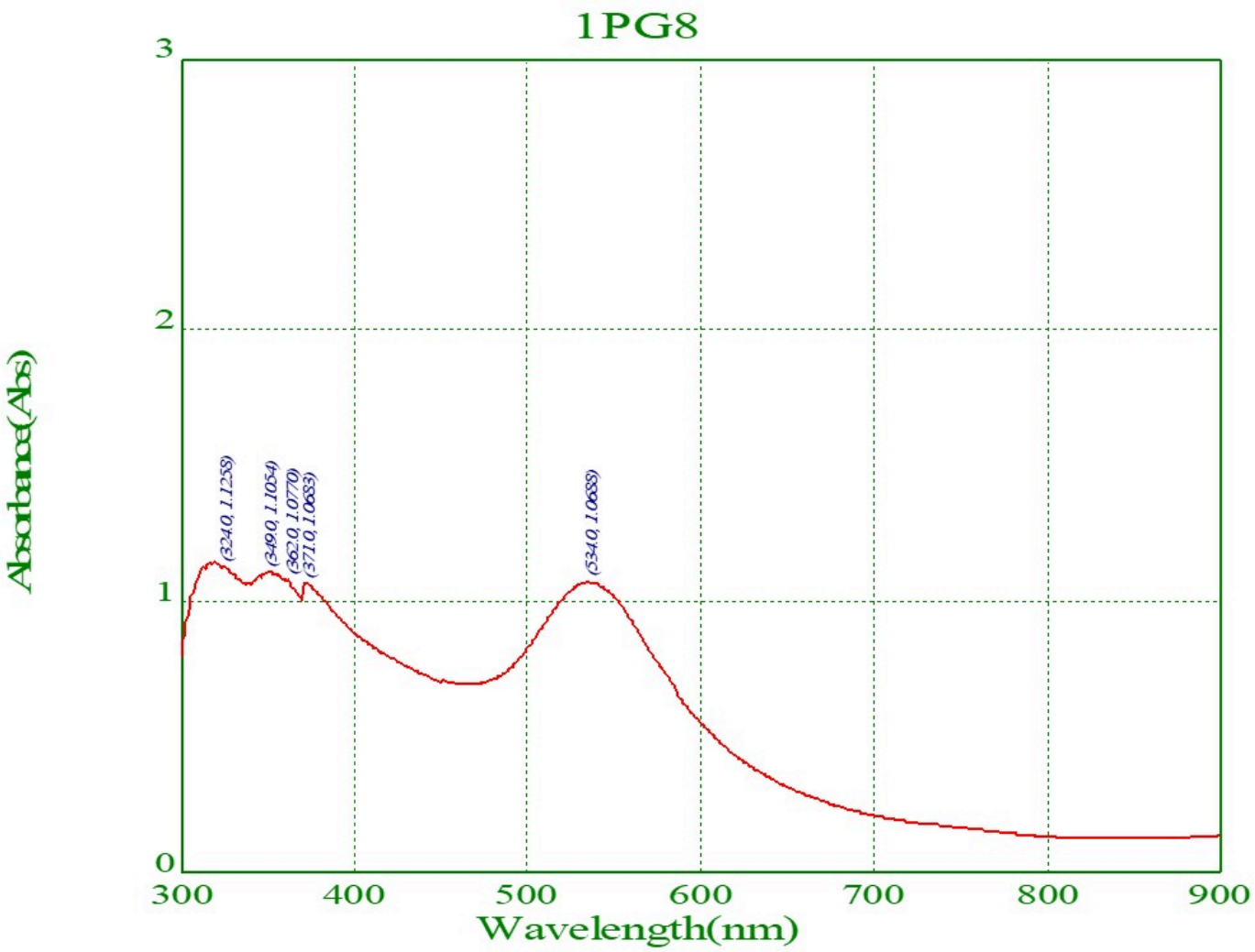

Figure 5

UV-Visible spectrum of AuNP's of *P. capitata* leaves part

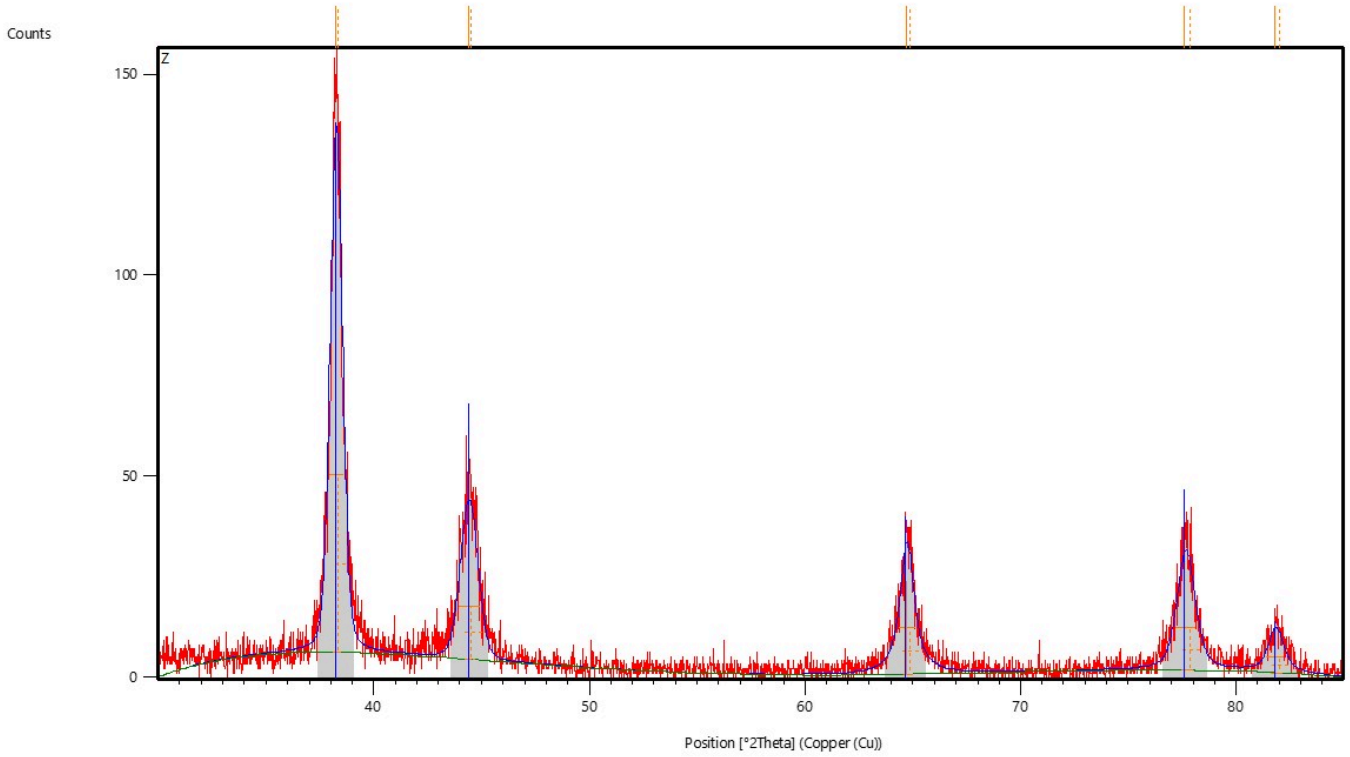

Figure 6

XRD spectra of synthesized AuNP's of *P. capitata* leaves part

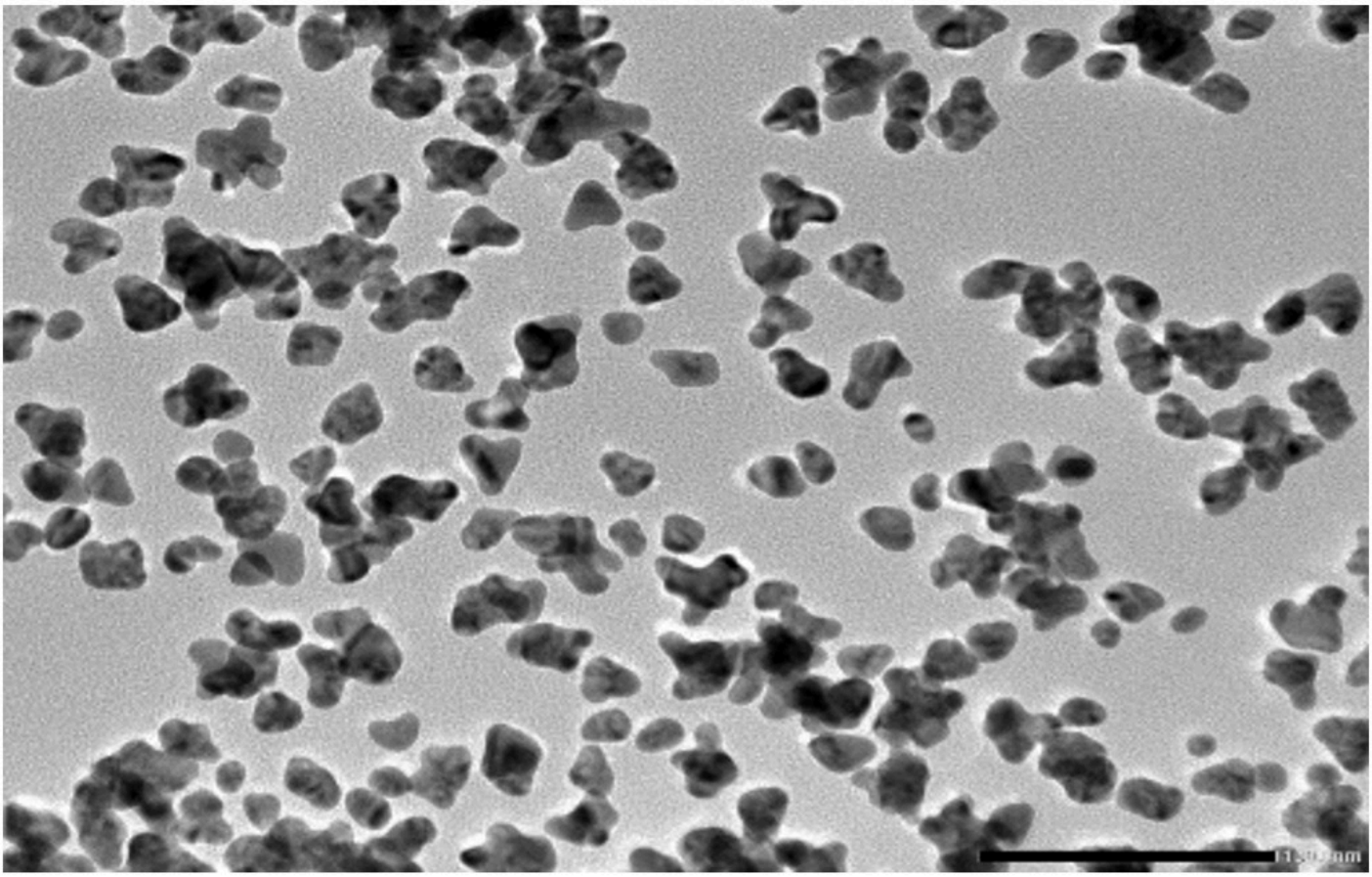

Figure 7

TEM image of synthesized AuNP's of *P. capitata* leaves part

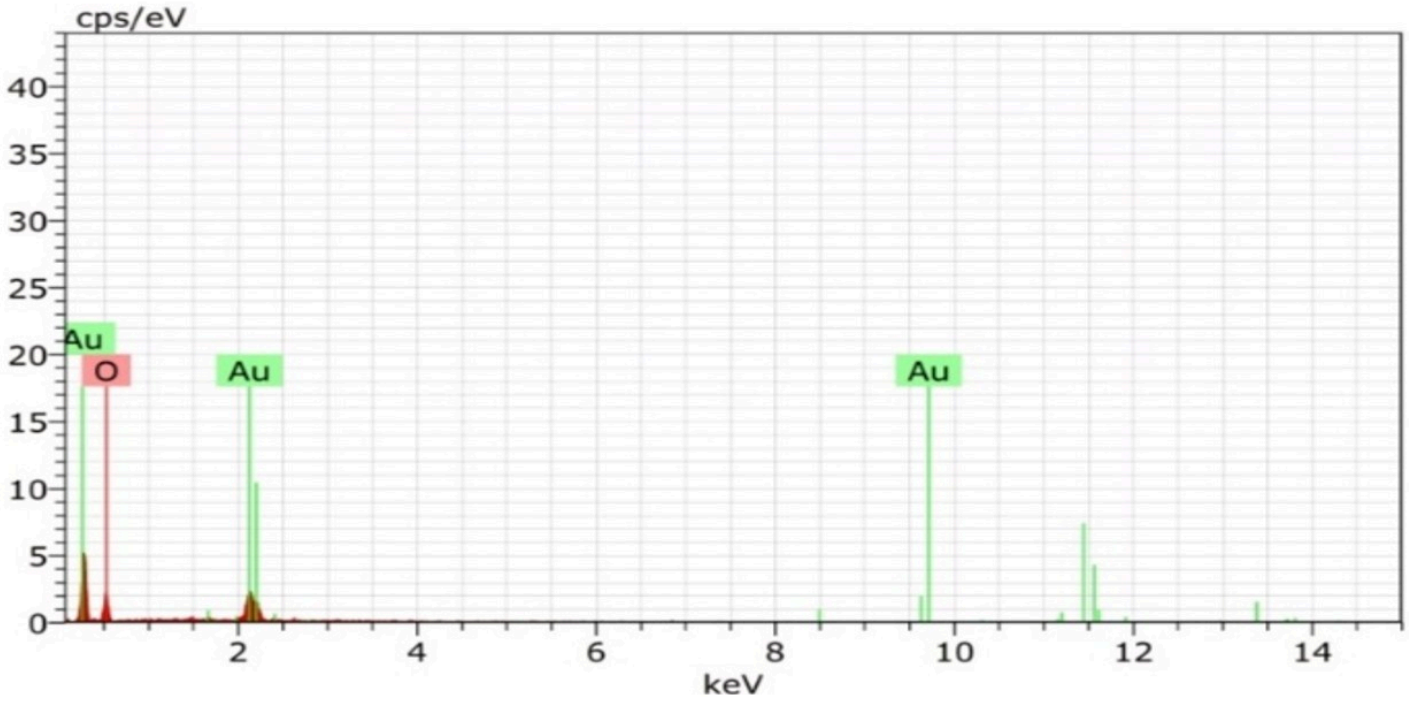

Figure 8

EDX spectrum of AuNP's of *P. capitata* leaves part

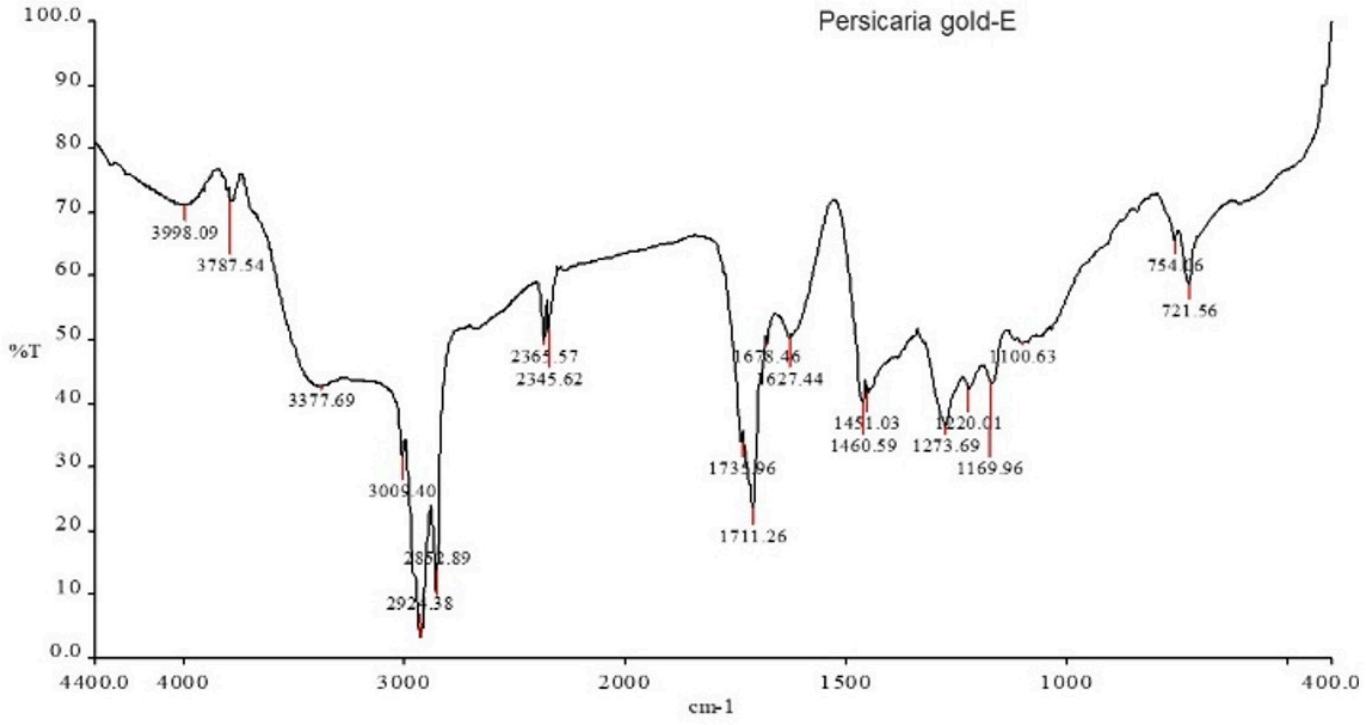

Figure 9

FTIR spectra of synthesized AuNP's *P. capitata* leaves part

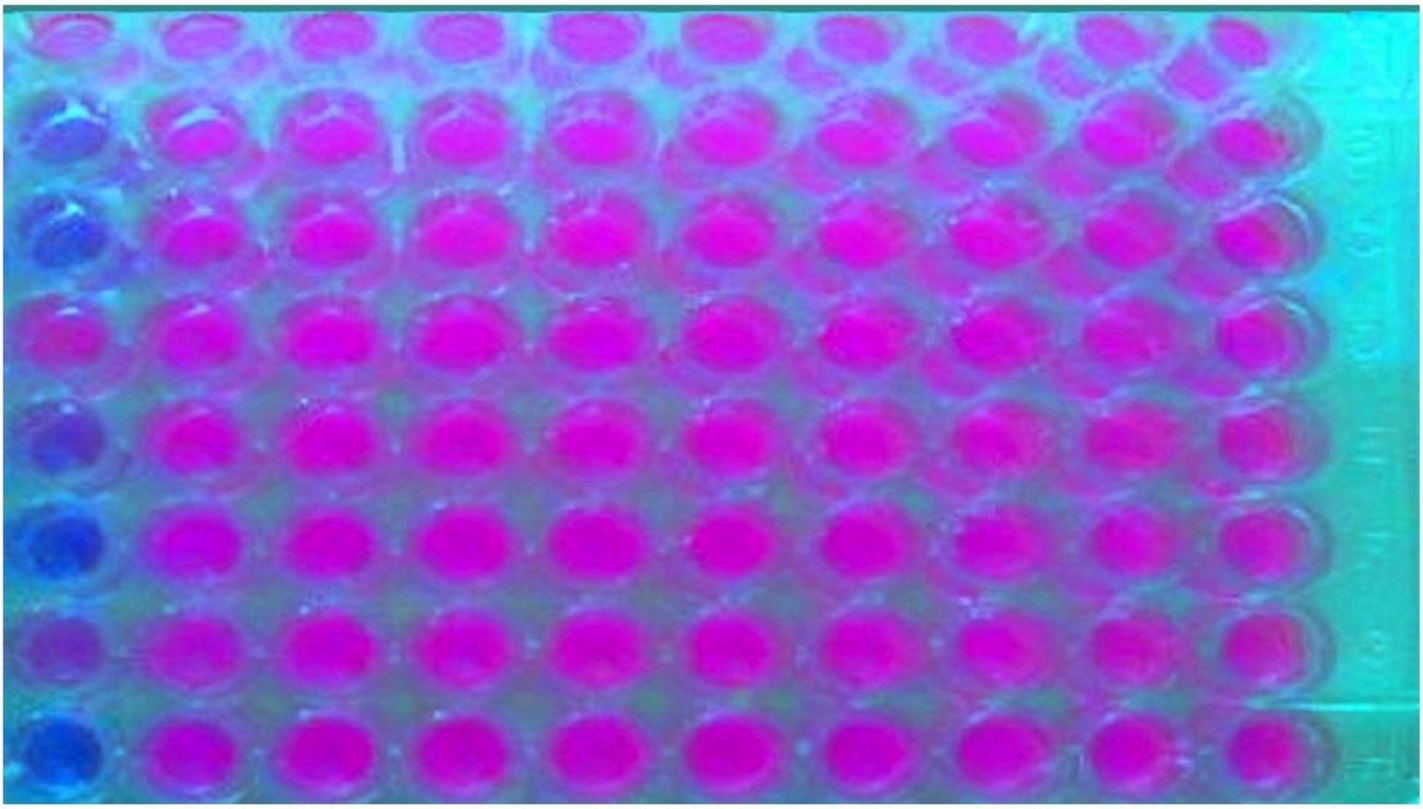

Figure 10

Viability of cells in cancer cell lines in titter plate as determined by Trypan blue assay (Pink coloured wells shows viability of the cells; Blue coloured wells show non-viable cells)

Figure 11

Antimicrobial activity of *P. capitata* (E) of gold nanoparticles against different bacterial strains.

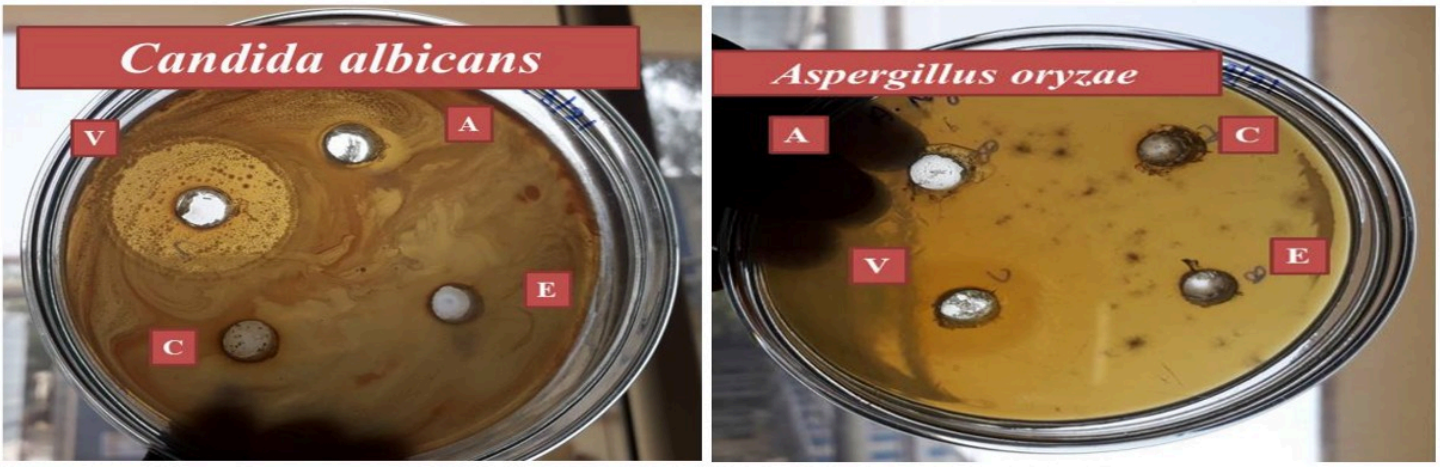

Figure 12

Antimicrobial activity of *P. capitata* (E) of gold nanoparticles against different fungal strains.